Preparation and Characterization of Flexible Asymmetric Supercapacitors Based on Transition-Metal-Oxide Nanowire/Single-Walled Carbon Nanotube Hybrid Thin-Film Electrodes

Po-Chiang Chen, Guozhen Shen, Yi Shi, Haitian Chen, and Chongwu Zhou*

Ming-Hsieh Department of Electrical Engineering, University of Southern California, Los Angeles, California 90089

ABSTRACT In the work described in this paper, we have successfully fabricated flexible asymmetric supercapacitors (ASCs) based on transition-metal-oxide nanowire/single-walled carbon nanotube (SWNT) hybrid thin-film electrodes. These hybrid nanostructured films, with advantages of mechanical flexibility, uniform layered structures, and mesoporous surface morphology, were produced by using a filtration method. Here, manganese dioxide nanowire/SWNT hybrid films worked as the positive electrode, and indium oxide nanowire/SWNT hybrid films served as the negative electrode in a designed ASC. In our design, charges can be stored not only *via* electrochemical double-layer capacitance from SWNT films but also through a reversible faradic process from transition-metal-oxide nanowires. In addition, to obtain stable electrochemical behavior during charging/discharging cycles in a 2 V potential window, the mass balance between two electrodes has been optimized. Our optimized hybrid nanostructured ASCs exhibited a superior device performance with specific capacitance of 184 F/g, energy density of 25.5 Wh/kg, and columbic efficiency of ~90%. In addition, our ASCs exhibited a power density of 50.3 kW/kg, which is 10-fold higher than obtained in early reported ASC work. The high-performance hybrid nanostructured ASCs can find applications in conformal electrics, portable electronics, and electrical vehicles.

KEYWORDS: metal oxide nanowires · single-walled carbon nanotubes · carbon nanotube films · supercapacitors · flexible energy storage devices

Electrochemical capacitors (so-called supercapacitors), with desirable properties of high power density (10 times more power than batteries), fast charging (with seconds), excellent cycling stability, small size, and light weight, have become some of the most promising candidates for next-generation power devices.[1−4] With characteristics complementary to those of rechargeable batteries and fuel cells, supercapacitors have been used in many applications, such as power back-up, pacemakers, air bags, and electrical vehicles.[5−7] Currently, most commercial supercapacitors are made of high-surface-area carbonaceous materials typically, with a specific capacitance of ~4 F/g, a power density of 3−4 kW/kg, and an energy density of 3−4 Wh/kg in both aqueous electrolyte and organic electrolyte, in which the weight of the whole system is considered.[8] However, these supercapacitors might not provide sufficient energy/power densities or efficiencies to fuel low-emission hybrid cars and trucks.

Therefore, the challenge for current supercapacitor technology is to improve the energy density without sacrificing the power density and the cycle life. According to the equation of $E = {}^1/_2CV^2$, obviously, the energy density can be improved by maximizing the device capacitance (C) and/or the cell voltage (V).[9] An efficient way to increase the cell voltage is to use organic electrolytes, since organic electrolytes usually provide a wider voltage window with better electrochemical stability than aqueous electrolytes. For instance, tetraethylammonium tetrafluoroborate ($TEABF_4$) in acetonitrile (AN) has been used as an electrolyte in supercapacitors, which allows the supercapacitors to be charged/discharged up to 2.0 or 2.3 V.[10] However, organic electrolytes are usually more expensive and less conductive than aqueous electrolytes ($\sigma_{LiPF_6:EC:DEC} \approx 10$ mS/cm; $\sigma_{1\ M\ Na_2SO_4} > 100$ mS/cm), which results in low specific capacitance and high equivalent series resistance in supercapacitors and precludes supercapacitors reaching high power density. In addition, AN is not environmentally friendly and can cause a toxic effect in human organs, which does not meet the requirement of "green electrolyte" for next-generation power devices. In this regard, aqueous-electrolyte-based supercapacitors are more

*Address correspondence to chongwuz@usc.edu.

Received for review April 20, 2010 and accepted July 14, 2010.

Published online July 26, 2010. 10.1021/nn100856y

attractive because they are highly safe, low-cost, and environmentally friendly.

An alternative approach to improve energy density is to develop hybrid electrochemical capacitors (so-called asymmetric supercapacitors, or ASCs),[11−13] which can also provide a wider operating potential window compared to symmetric supercapacitors. For an ASC, the active material used in one electrode is usually different from that used in the other electrode in a cell system. For instance, ruthenium oxide (RuO_2) can be used as the positive electrode,[14] while activated carbon (AC) can work as the negative electrode in an ASC.[15] Moreover, ASCs can make use of the different potential windows of the two electrodes to increase the maximum operation voltage of the aqueous electrolyte in the cell system, which results in an improved specific capacitance and energy density. In comparison to conventional electrical double-layer capacitors (EDLCs), Qu *et al.* reported the use of manganese dioxide as the positive electrode and AC as the negative electrode in an ASC, with operation voltage of 1.8 V, energy density of 28.4 Wh/kg, and power density of 150 W/kg in an aqueous electrolyte.[16] Due to the improved energy density, much attention has been paid to such transition-metal-oxide/AC ASCs. Yuan *et al.* presented an ASC built on two different transition-metal-oxide materials, and the device exhibited energy density of 23 Wh/kg and improved power density of 1.4 kW/kg at a high discharging current of 25 mA/cm^2.[17] However, none of the reported devices could supply a power density comparable to that of single-walled carbon nanotube (SWNT) EDLCs (23 kW/kg) in an aqueous gel electrolyte.[18] This can be attributed to the poor conductance of the transition-metal-oxide-based electrodes, which decreases the power density of the ASCs.

To address this issue, we have developed an easy and efficient method to improve the conductivity of transition-metal-oxide-based electrodes by integrating transition-metal-oxide nanowires together with SWNTs to form hybrid nanostructured films, which have been applied as electrodes in flexible and transparent supercapacitors.[19] In our early work, the incorporation of transition-metal-oxide nanowires contributed pseudocapacitance to SWNT thin-film EDLCs, thus improving the device performance in terms of specific capacitance and power density. In the work described herein, using a similar concept, we prepared hybrid nanostructured thin-film electrodes by using two different transition-metal-oxide nanowires, including manganese dioxide (MnO_2) nanowires and indium oxide (In_2O_3) nanowires, together with SWNTs and fabricated hybrid nanostructured ASCs. In this asymmetric cell system, MnO_2 nanowire/SWNT hybrid films served as the positive electrode, while In_2O_3 nanowire/SWNT hybrid films functioned as the negative electrode with a neutral electrolyte. In order to obtain a stable 2 V operation potential for the hybrid nanostructured ASCs, the mass balance between the two electrodes of the cell system has been optimized. The optimized hybrid nanostructured ASCs operated stably up to 2 V with specific capacitance of 184 F/g, power density of 50.3 kW/kg, and energy density of 25.5 Wh/kg. In comparison to the early reported ASCs, our hybrid nanostructured ASCs exhibit better power density, which can be attributed to the integration of SWNTs. In addition, our design not only takes full advantage of the electrical double-layer capacitance from SWNTs and the pseudocapacitance from transition-metal-oxide nanowires but also improves the conductivity of transition-metal-oxide nanowire films, which leads to high energy density and high power density of our ASCs. Furthermore, SWNT films also worked as current-collecting electrodes, which further reduced the total device weight by eliminating the need for metal current-collecting electrodes used in conventional supercapacitors.

RESULTS AND DISCUSSION

Characterizations of Indium Oxide Nanowires and Manganese Oxide Nanowires. Figure 1a shows a typical scanning electron microscopy (SEM) image of as-grown MnO_2 nanowires with typical length of ~2−3 μm and diameter of ~20 nm on average. These nanowires have smooth surfaces without any amorphous coating and have extremely uniform diameters, which can be easily observed in the low-magnification transmission electron microscopy (TEM) image (Figure 1b). In addition, there is no noticeable dislocation or defect in MnO_2 nanowires, and the corresponding high-resolution (HR)-TEM image, shown in Figure 1c, exhibits a perfect single-crystalline structure with a very good lattice fringe, corresponded to a *d*-spacing of 0.31 nm in the β-phase MnO_2 (β-MnO_2) crystal structure.[20] To further evaluate the crystalline structure, Figure 1d shows the result of X-ray diffraction (XRD) measurement. The XRD pattern also confirmed the crystalline structure of as-grown nanowires to be β-MnO_2 nanowires, which have tetragonal symmetry with *P*42/*mnm* space group and lattice constants of $a = 4.388$ nm and $c = 2.865$ nm (JCPDS data, PDF-01-072-1984). Furthermore, there is no extra peak observed in the XRD spectrum, which confirms the highly crystalline nature of the MnO_2 nanowires and is in agreement with the HR-TEM observations. Figure 1e displays the SEM image of chemical vapor deposition (CVD) synthesized In_2O_3 nanowires which are 10−100 μm long with diameters of 50−100 nm on average. Similar to MnO_2 nanowires, both low-magnification TEM (Figure 1f) and HR-TEM (Figure 1e) suggest that each In_2O_3 nanowire has a perfect single-crystalline structure without any noticeable dislocations or defects. The interspacing between planes is 0.505 nm, corresponding to the (200) plane in the body-centered cubic (bcc) In_2O_3 nanowire crystal structure, with a lattice constant of $a = 1.01$ nm.[21,22] Although the XRD pattern shown in Figure 1h exhibits two extra Au

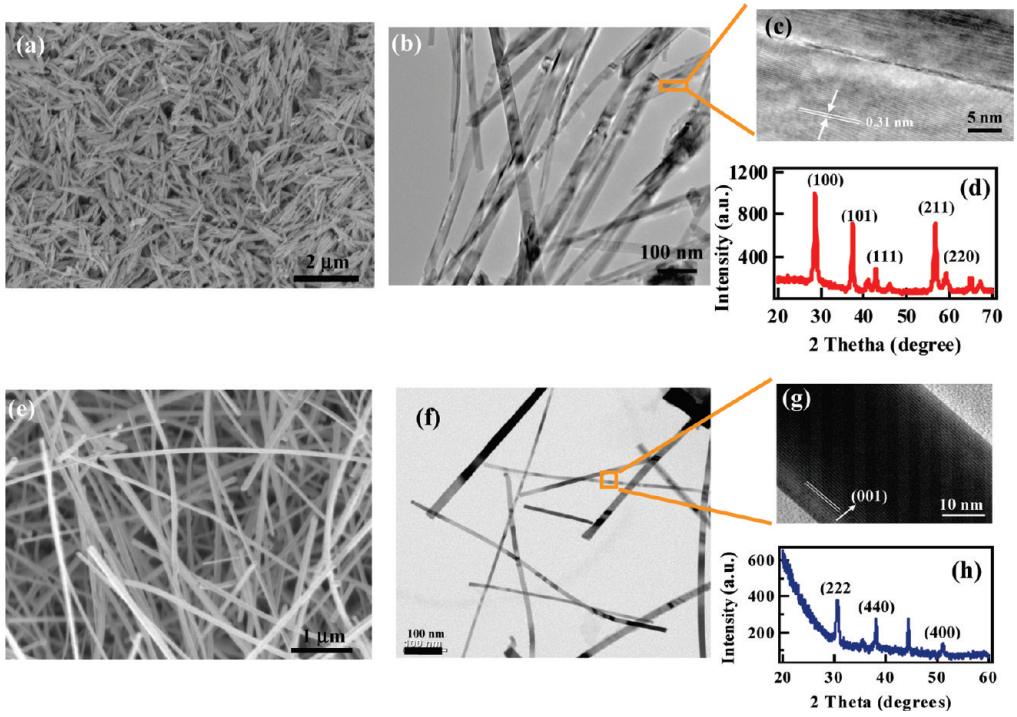

Figure 1. (a) SEM image of β-MnO_2 nanowires with diameter of 20 nm and length of 2−3 μm on average. (b) TEM image of β-MnO_2 nanowires. (c) High-resolution TEM of a β-MnO_2 nanowire. (d) A typical XRD spectrum of as-grown β-MnO_2 nanowires. (e) SEM images of In_2O_3 nanowires with diameter of 60 nm and length of 10−100 μm on average. (f) TEM image of In_2O_3 nanowires. (g) High-resolution TEM of an In_2O_3 nanowire. (h) A typical XRD spectrum of as-grown In_2O_3 nanowires.

peaks due to the existence of Au catalysts, the XRD patterns also indicate that these nanowires exhibit high crystalline quality.[20]

Fabrication and Characterizations of Hybrid Nanostructured Films. To produce hybrid nanostructured films, the as-grown transition-metal-oxide nanowires were sonicated in isopropyl alcohol (IPA) solutions and then dispersed on a SWNT film/anodic aluminum oxide (AAO) membrane to form transition-metal-oxide nanowire/SWNT hybrid films by a filtration method. As the suspension went through the SWNT film/filtration membrane, the nanowires were trapped on the SWNT films and formed an intertwined mesh. The "hybrid nanostructured thin films" were gently peeled off, while the trapped nanowire/SWNT films dried. These hybrid nanostructured films were characterized by mechanical flexibility, uniform layered structures, and mesoporous surface morphology. Figure 2a shows a schematic diagram of an ASC built on two different hybrid nanostructured films. As one can easily observe, the asymmetric cell system is composed of a nitrocellulose film as the separator, a MnO_2 nanowire/SWNT film as the positive electrode, an In_2O_3 nanowire/SWNT film as the negative electrode, and aqueous solution as the electrolyte. Figure 2b shows a typical MnO_2 nanowire/SWNT hybrid film electrode. MnO_2 nanowires are uniformly coated on SWNT films. To check the interface between the SWNT networks and MnO_2 nanowire mesh, we intentionally stretched a MnO_2 nanowire/SWNT hybrid film electrode. Uniform SWNT networks underneath the MnO_2 nanowire films can be clearly observed in the inset of Figure 2b, and the MnO_2 nanowires are well-distributed and form a homogeneous film on SWNT films. Similar to the MnO_2 nanowire/SWNT hybrid films, Figure 2c shows a well-dispersed In_2O_3 nanowire mesh on SWNT networks forming a layer-by-layer structure. The inset displays the SWNT networks below the In_2O_3 nanowire films. By using the filtration method, we produced conformal, binder-free, all-nanostructured-materials hybrid nanostructured films with highly tunable surfaces, which allows aqueous electrolytes to fully wet the nanowire mesh and the SWNTs. The well-distributed oxide nanowire films maintained good contact with SWNTs and provided a good electrical conduction pathway for charge transportation. In addition, we note that uniformly dispersed transition-metal-oxide nanowire films and a layer-by-layer structure are critical in this study, since charges can uniformly distribute on each electrode and the cell voltage can split equally on both electrodes.

Electrochemical Characterizations of Hybrid Nanostructured Films. Electrochemical measurements were carried out with a potentiostat/galvanostat (Princeton Applied Research model 263) in 1 M Na_2SO_4 electrolyte. Galvanostatic (GV) charging/discharging measurements were used to determine the specific capacitance (C_{sp}), power density, and internal resistance (IR) of the devices in a two-electrode configuration. Cyclic voltammetery (CV) measurements were performed to evaluate the stability and the electrochemical behavior of our hybrid

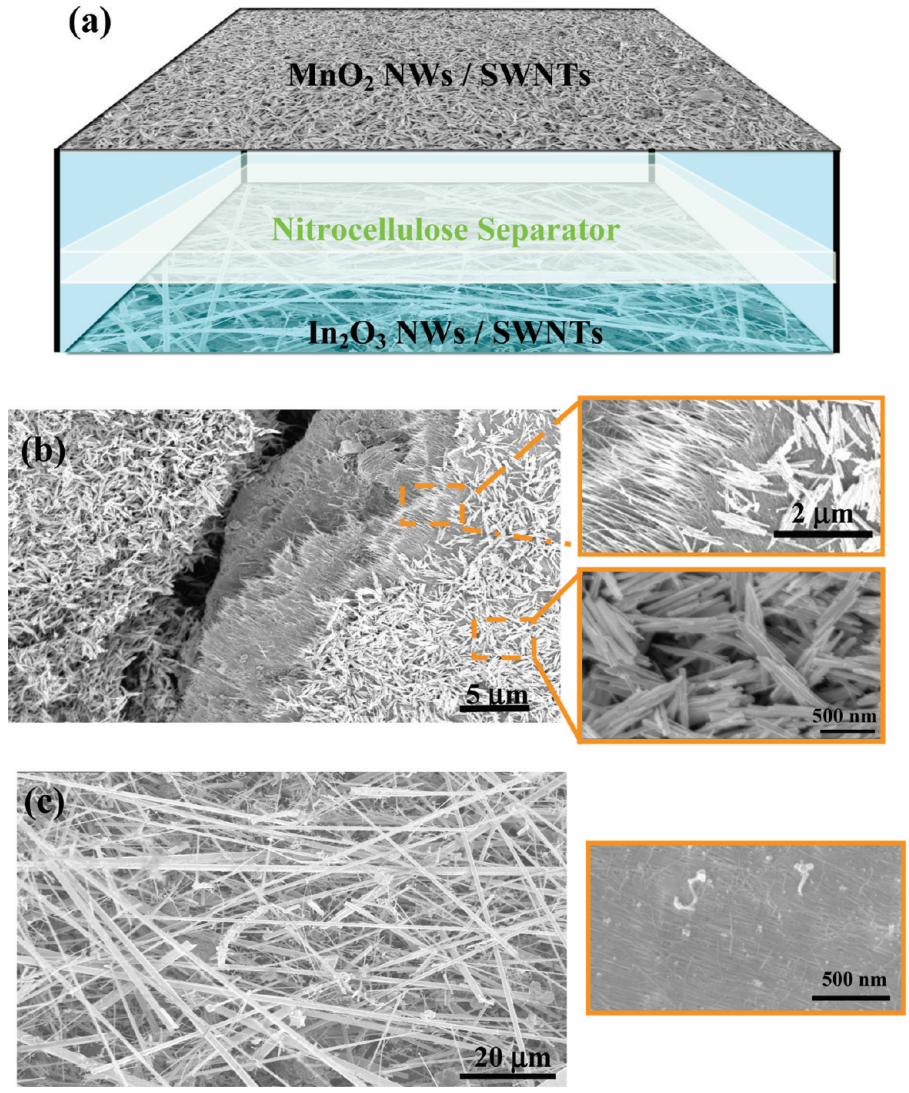

Figure 2. (a) Schematic diagram of an ASC composed with a MnO_2 nanowire/SWNT hybrid film as a cathode electrode and and In_2O_3 nanowire/SWNT hybrid film as an anode electrode. (b) A scratched MnO_2 nanowire/SWNT hybrid film. Insets: (top) SWNT films can be clearly observed underneath MnO_2 nanowire networks; (bottom) uniform MnO_2 nanowire network above SWNT films. (c) An as-fabricated In_2O_3 nanowire/SWNT hybrid film. Inset: SWNT films underneath In_2O_3 nanowires work as current-collecting electrodes.

nanostructured films under different potential windows from −0.6 to 0.8 V in a three-electrode configuration. A hybrid nanostructured film, an Ag/AgCl (saturated NaCl) assembly, and a platinum wire were used as the working electrode, the reference electrode, and the counter electrode, respectively. The electrochemical performance was tested without removal of oxygen from the solution.[23] The potential range of MnO_2 and In_2O_3 hybrid nanostructured films extends from 0.0 to 0.8 V and −0.6 to 0.2 V *vs* Ag/AgCl, respectively, while In_2O_3 nanowires are more stable at more negative potentials. The CV results of SWNT bulky papers, MnO_2 nanowire/SWNT hybrid films, and In_2O_3 nanowire/SWNT hybrid films in the aqueous electrolyte are presented in Figure 3. Figure 3a shows the results of CV measurements of SWNT bulky papers with different scan rates of 5 and 20 mV/s around potentials of 0.0 and 0.8 V. The rectangular shape of these curves reveals a good electrical double-layer capacitance behavior of our SWNT bulky papers. The cyclic voltammograms of MnO_2 nanowire/SWNT hybrid films with scan rates of 5, 20, 50, and 100 mV/s can be found in Figure 3b, which shows a quasi-rectangular shape of these curves. As is well known, MnO_2 is considered to be a promising electrode material, exhibiting ideal capacitive behavior in a mild aqueous electrolyte with a stable potential range up to 1.2 V.[13] The charge-storage mechanism of MnO_2 is still controversial.[23,24] For crystalline MnO_2, the mechanism might can be attributed to the intercalation/extraction of protons (H_3O^+) or alkali cations (Na^+) into/out of the oxide nanowires with concomitant reduction/oxidation of the Mn ions and can be expressed as follows:[24]

$$MnO_2 + M^+ + e^- \leftrightarrow MnOOM \quad (M^+ = Na^+ \text{ or } H_3O^+) \quad (1)$$

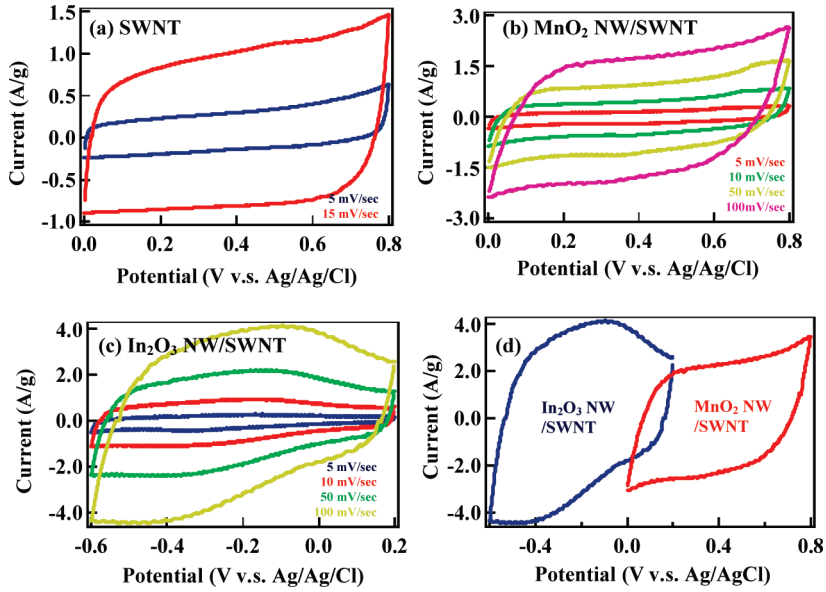

Figure 3. Cyclic voltammetery in a three-electrode configuration with different nanostructured thin-film electrodes of (a) a bare SWNT thin-film electrode, (b) a MnO_2 nanowire/SWNT hybrid film electrode, and (c) an In_2O_3 nanowire/SWNT hybrid film electrode in 1 M Na_2SO_4 electrolyte with different scan rates ranging from 5 to 100 mV/s. (d) Comparative cyclic voltammetery using MnO_2 nanowire/SWNT hybrid film and In_2O_3 nanowire/SWNT hybrid film as active electrodes. The scan rate is 100 mV/s.

The quasi-rectangular shapes are close to the behavior of EDLCs, even though the Faradaic process dominates the electrochemical behavior of MnO_2 nanowire networks in an aqueous electrolyte.[16] In addition, the SWNT films underneath the MnO_2 nanowire networks also contributed electrical double-layer capacitance, which might influence the CV shapes of MnO_2 nanowire/SWNT hybrid films.

Figure 3c displays the cyclic voltammograms of In_2O_3 nanowire/SWNT hybrid films with scan rates of 5, 20, 50, and 100 mV/s. Similar to the MnO_2 nanowire/SWNT hybrid films, the In_2O_3 nanowire/SWNT films exhibit a quasi-rectangular shape with Faradaic process contributed by the In_2O_3 nanowires.[25] In comparison to Figure 3a, as one can easily see, the cyclic voltammograms of the two hybrid nanostructured films are quite different due to the Faradaic process contributed by the transition-metal-oxide nanowires. The specific capacitance of those active materials can be obtained *via* the following equation:[26,27]

$$C(\mathrm{F/g}) = \frac{i}{\nu}\left(\frac{1}{m}\right) \qquad (2)$$

where ν is the scan rate, i is the corresponding current of the applied voltage, and m is the weight of the active materials. With this equation, the specific capacitance of SWNT bulky paper is calculated to be about 80 F/g, that of MnO_2 nanowire/SWNT hybrid film is 253 F/g, and that of In_2O_3 nanowire/SWNT hybrid film is 201 F/g.

By expressing the total cell voltage as the sum of the potential range of MnO_2 nanowire/SWNT hybrid film and In_2O_3 nanowire/SWNT hybrid film, we are able to estimate that the hybrid nanostructured ASCs can be operated up to 1.4 V. Figure 3d shows the cyclic voltammograms obtained in a three-electrode cell from MnO_2 nanowire/SWNT hybrid film electrode and In_2O_3 nanowire/SWNT hybrid film electrode in 1 M Na_2SO_4 electrolyte. It is easy to observe that the MnO_2 nanowire/SWNT hybrid film has a stable electrochemical behavior in positive polarization and the In_2O_3 nanowire/SWNT hybrid film has a stable electrochemical behavior in negative polarization. Hence, in order to obtain a capacitor operating in a 1.4 V voltage window, it is necessary to control the experimental conditions for the MnO_2 nanowire/SWNT hybrid film to work in the potential window range from 0.2 to 0.8 V and for the In_2O_3 nanowire/SWNT hybrid film to work in the potential window range from −0.6 to 0.2 V, which will ensure a safe performance of both electrodes during long cycling. In this way, we can avoid the decomposition of aqueous electrolyte at 1 V that occurs in a symmetric cell system. In addition, more negative potential (for reduction) and positive potential (for oxidation) can be achieved, since both the hydrogen and oxygen evolution reactions are presumably kinetically limited on these transition-metal-oxide nanowires and SWNTs. As a result, the operation window of MnO_2 nanowires can extend from −0.1 to 1.2 V and that of In_2O_3 nanowires from −1.0 to 0.2 V *vs* Ag/AgCl in 1 M Na_2SO_4 electrolyte.

Moreover, unlike a symmetric supercapacitor, in which the applied voltage can split equally between the two electrodes due to using the same material and having the same mass in each electrode, in ASCs, the voltage split depends on the capacitance of the active material in each electrode. The capacitance is usually related to the mass and the specific capacitance of the active material.[13] Thus, in order to split voltage equally,

we have to optimize the mass balance between the two electrodes in our cell system following the relationship $q_+ = q_-$, where q_+ means the charges stored at the positive electrode and q_- means the charges stored at the negative electrode.[11] The stored charge can be expressed by the following equation:[11]

$$q = C_{sp} m \Delta E \quad (3)$$

where ΔE is the potential range of the charging/discharging process and m is the mass of each electrode. Since the mass loading of SWNTs in each electrode is the same, the optimal mass ratio between the electrodes should be $m_{MnO_2}/m_{In_2O_3} = 0.74$ in the hybrid nanostructured asymmetric cell system.

Asymmetric Hybrid Nanostructured Supercapacitors. Figure 4a shows the cyclic voltammograms at different cell voltages for a hybrid nanostructured ASC with optimal mass ratio between two electrodes in 1 M Na_2SO_4 electrolyte. In the designed cell, the weight of MnO_2 nanowires is 0.46 mg and that of In_2O_3 nanowires is 0.62 mg. With a scan rate of 20 mV/s, the hybrid nanostructured supercapacitor shows an ideal capacitive behavior with quasi-rectangular CV curves, even at a potential window up to 2.0 V in 1 M Na_2SO_4 electrolyte. The cell maintained an ideal capacitive behavior even at the high scan rate of 100 mV/s, which exhibits the desirable fast-charging/discharging property for power devices, as shown in Figure 4b. Figure 4c displays 10 cycles of galvanostatic charging/discharging curves for an ASC with a constant current of 2 mA/cm^2 in the potential range between 0.01 and 2.01 V. The symmetry of the charging and discharging characteristics shows good capacitive behavior. The specific capacitance has been evaluated from the charging/discharging curves according to the following equation:[19]

$$C_{sp} = \left(\frac{I}{-dV/dt}\right)\left(\frac{1}{m_+} + \frac{1}{m_-}\right) \quad (4)$$

where I is the applied discharging current, m_+ and m_- are the masses of the positive and negative electrodes, respectively, and the dV/dt is the slope of the of discharge curve after IR drop. The power density and energy density can be calculated using the following equations:[11]

$$P = \frac{V^2}{4RM} \quad (5)$$

$$E = \frac{1}{2}CV^2 = \frac{1}{8}MC_{sp}V^2 \quad (6)$$

where V is the applied voltage, R is the equivalent series resistance (ESR), M is the total mass of the hybrid nanostructured film electrodes, and C is the total capacitance of the hybrid nanostructured ASC ($C_{sp} = 4C/M$).[28] The calculated specific capacitance of the hybrid nanostructured ASC is about 184 F/g, while the power density and energy density were improved to 50.3 kW/kg and 25.5 Wh/kg, respectively. We also carried out the GV measurements for SWNT symmetric supercapacitors; the results are given in the Supporting Information. The specific capacitance was merely 80 F/g, with power density of 11.4 kW/kg and energy density of 4 Wh/kg. We further investigated the device performance of hybrid nanostructured ASCs and SWNT symmetric supercapacitors by using different charging/discharging currents. Figure 4d shows the specific capacitance of a SWNT symmetric supercapacitor and

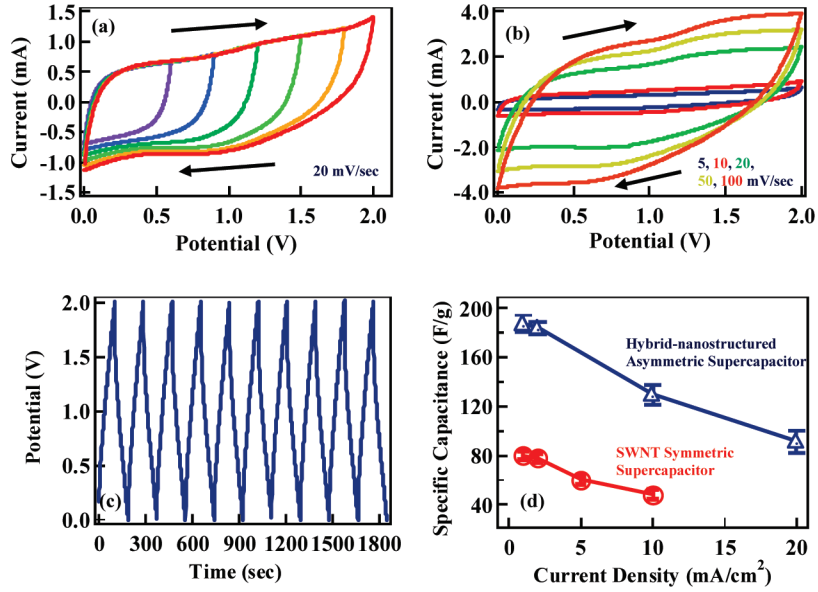

Figure 4. Cyclic voltammograms of an optimized hybrid nanostructured ASC in 1 M Na_2SO_4 electrolyte with a scan rate of 20 mV/s (a) and with different scan rates of 5, 10, 20, 50, 75, and 100 mV/s (b). (c) Galvanostatic charging/discharging curves measured with a current density of 2 mA/cm^2 for an optimized hybrid nanostructured ASC in 1 M Na_2SO_4 electrolyte. (d) A comparison of the specific capacitance of a hybrid nanostructured ASC and a SWNT symmetric supercapacitor with different discharging currents of 1, 2, 5, 10, and 20 mA/cm^2.

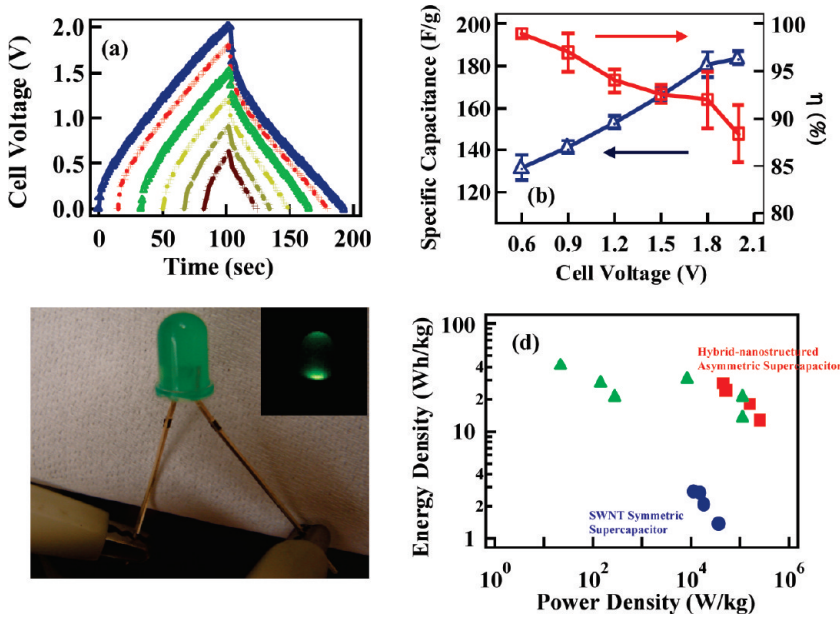

Figure 5. (a) Galvanostatic charging/discharging curves (I = 2 mA/cm^2) of an optimized asymmetric nanostructured supercapacitor in 1 M Na_2SO_4 electrolyte. Cyclic voltammograms were obtained on an optimized asymmetric nanostructured supercapacitor in 1 M Na_2SO_4 electrolyte with a scan rate of 20 mV/s. (b) Coulombic efficiency and specific capacitance of a hybrid nanostructured ASC in 1 M Na_2SO_4 electrolyte *vs* different cell voltage. (c) Photo image of a green LED connected with the hybrid nanostructured ASC before/after discharging (inset). (d) A Rogone plot showing that the hybrid nanostructured ASCs outperform the SWNT symmetric supercapacitors and early ASC data reported in the literature.

a hybrid nanostructured ASC as a function of the different discharging current density. The decrease in the specific capacitance of both supercapacitors can be attributed to the decrease of the utilization efficiency of active materials with increasing discharging current. The hybrid nanostructured ASCs showed specific capacitance of 90 F/g, even at a discharging current of 20 mA/cm^2.

Figure 5a shows the galvanostatic charging/discharging curves of one hybrid nanostructured ASC with different maximum cell voltages. The specific discharge capacitance was improved with increasing cell voltage, and the charging/discharging behavior was capacitive with symmetric charge−discharge curves up to 1.5 V. However, with increasing cell voltage, noncapacitive behavior with nonsymmetric charge−discharge curve was found. Therefore, to determine the optimal cell voltage, the Coulombic efficiency should be evaluated, according to the following equation:[17]

$$\eta = \frac{q_d}{q_c} \times 100\% \qquad (7)$$

where q_d and q_c are the total amounts of discharge and charge of the capacitor obtained from the galvanostatic experiments, exhibited in Figure 5a. Figure 5b represents the Coulombic efficiency and the average specific discharge capacitance of both electrodes as a function of the cell voltage in five hybrid nanostructured ASCs. Whereas the capacitance increases with the cell voltage, the Coulombic efficiency decreases significantly when the voltage is above 1.8 V. This might be attributed to the splitting of water, since oxide nanowires did not completely cover the SWNT films. More layers of oxide nanowires may help the surface coverage and eliminate the water-splitting phenomenon.

To show the practical applications of hybrid nanostructured ASCs, we connected one hybrid nanostructured ASC with a green light-emitting diode (LED) (driving voltage, 1.5 V) and successfully lighted it, which can be observed in the inset of Figure 5c. To highlight the superior device performance of hybrid nanostructured ASCs, Figure 5d shows the Ragone plots of SWNT symmetric supercapacitors and hybrid nanostructured ASCs. All the data were calculated on the basis of the total mass of active materials of two electrodes. It can be seen that the hybrid nanostructured ASCs exhibit much higher energy density and power density than the SWNT symmetric supercapacitors. In addition, in comparison to previously reported asymmetric configurations,[14,16,17,29,30] our hybrid nanostructured ASCs display comparable energy density and higher power density, which can be attributed to the integration of transition-metal-oxide nanowires and SWNTs to form a binder-free, hybrid nanostructured thin-film electrodes, which thus improves the conductivity of electrodes and power density of asymmetric cells.

In summary, we have developed a simple and efficient way to obtain flexible, mesoporous, and uniform hybrid nanostructured thin-film electrodes for supercapacitor study. Our hybrid nanostructured asymmetric supercapacitors exhibited superior device performance over SWNT symmetric supercapacitors in terms of operation voltage, specific capacitance, energy density,

and power density. The superior performance can be attributed to (1) the enhanced charge storage contributed by electrical double-layer capacitance from SWNT films and pseudocapacitance from transition-metal-oxide nanowires, (2) good conductivity as a result of using SWNTs as conductivity agent in our design, and (3) the optimized mass balance, which allowed us to operate the devices in a 2 V potential window with stable electrochemical behavior. In addition, the total weight of our devices is further reduced because they do not require metal current-collecting electrodes and binders. The optimized ASCs in aqueous electrolyte have shown improved device performance in specific capacitance of 184 F/g, power density of 50.3 kW/kg, and energy density of 25.5 Wh/kg. The high-performance asymmetric supercapacitors can be applied in conformal electronics, portable electronics, and electrical vehicles.

METHODS

Preparation of Carbon Nanotube Films. The fabrication of hybrid nanostructured asymmetric supercapacitors began with the preparation of functionalized carbon nanotube (CNT) solutions. The details can be found in our early work.[31] In brief, arc-discharge carbon nanotubes (P3 nanotubes from Carbon Solutions Inc.) were mixed with 1 wt % aqueous sodium dodecyl sulfate (SDS) in distilled water to make a highly dense SWNT suspension with a typical concentration of 0.1 mg/mL. The addition of SDS surfactants further improves the solubility of SWNTs by sidewall functionalization. This SWNT solution was then ultrasonically agitated using a probe sonicator for ~20 min, followed by centrifugation to separate out undissolved SWNT bundles and impurities. To make a uniform SWNT thin-film electrode, the as-prepared SWNT suspension was filtered through a porous alumina filtration membrane (pore size, 200 nm; Whatman). As the solvent went through the membrane, SWNTs were trapped on the membrane surface and formed a homogeneous entangled network. After the filtration, a significant amount of distilled water was applied to remove the remaining SDS surfactant. During the trapping, the SWNT film became dry; the "bulky paper" thus formed was gently peeled off from the filtration membrane, which can be observed in Figure S-1 in the Supporting Information. The mass of as-fabricated SWNT bulky papers and hybrid nanostructured films was determined by a microbalance after filtrations. Typical mass loading of a 2-in.-diameter SWNT bulky paper was about ~8 mg, with a film thickness of 2.2 μm and sheet resistance of 13−16 Ω/square, which is comparable to that of early reported SWNT networks.[32,33] The electrode size used in this work was about 0.5 cm^2.

Synthesis of Metal Oxide Nanowires. MnO_2 nanowires were synthesized by using a so-called hydrothermal method reported elsewhere.[34] In brief, $Mn(CH_3COO)_2 \cdot 4H_2O$ and $Na_2S_2O_8$ (99.999%, Sigma Aldrich) were dissolved in 100 mL of distilled water with a molar ratio of 1:1 at room temperature and stirred by using a magnetic stirrer to form a clear and homogeneous solution. The mixed solution was then transferred to a 130 mL Teflon-lined stainless steel autoclave and heated at 120 °C for 12 h in an electrical oven for hydrothermal reactions. After the reaction, the products were washed with deionized water and ethanol to remove the sulfate ions and other remainders by filtration. The products were then dried in a vacuum oven at 100 °C for 12 h.

In_2O_3 nanowires were synthesized by using a thermal CVD method. A 5 nm gold film was deposited on Si/SiO_2 substrates as catalysts using an e-beam evaporator, followed by annealing at 700 °C for 30 min. The substrates were then placed into a quartz tube at the downstream position of a furnace, while stoichiometric In_2O_3 powders (99.99%, Alfa-Aesar) mixed with graphite powders were utilized as precursor and also placed at the center of a furnace. During the growth, the quartz tube was maintained at a pressure of 1 atm and a temperature of 900 °C, with a constant flow of 120 sccm. The typical reaction time was about 50 min. The as-grown nanowires were characterized by using field-emission scanning electron microscopy (FESEM, Philips S-2000), high-resolution transmission electron microscopy (HR-TEM, JEOL 100-CX), and X-ray diffractometer (XRD).

Acknowledgment. We acknowledge financial support from the National Science Foundation (CCF 0726815 and CCF 0702204).

Supporting Information Available: Fabrication details and electrochemical characterizations of SWNT thin-film electrodes and SWNT symmetric supercapacitors. This material is available free of charge *via* the Internet at http://pubs.acs.org.

REFERENCES AND NOTES

1. Winter, M.; Brodd, R. J. What Are Batteries, Fuel Cells, and Supercapacitors. *Chem. Rev.* **2004**, *104*, 4245–4269.
2. Simon, P.; Gogotsi, Y. Materials for Electrochemical Capacitors. *Nat. Mater.* **2008**, *7*, 845–854.
3. Pushparaj, V. L.; Shaijumon, M. M.; Kumar, A.; Murugesan, S.; Ci, L.; Vajtai, R.; Linhardt, R. J.; Nalamasu, O.; Ajayan, P. M. Flexible Energy Storage Devices Based on Nanocomposite Paper. *Proc. Natl. Acad. Sci. U.S.A.* **2007**, *104*, 13574–13577.
4. Arico, A. S.; Bruce, P.; Scrosati, B.; Tarascon, T.-M.; Schalkwijk, W. V. Nanostructured Materials for Advanced Energy Conversion and Storage Devices. *Nat. Mater.* **2005**, *4*, 366–377.
5. Futaba, D. N.; Hata, K.; Yamada, T.; Hiraoka, T.; Hayamizu, Y.; Kakudate, Y.; Tanaike, O.; Hatori, H.; Yumura, M; Iijima, S. Shape-Engineerable and Highly Densely Packed Single-Walled Carbon Nanotubes and Their Application as Super-Capacitor Electrode. *Nat. Mater.* **2006**, *5*, 987–994.
6. Liu, J.; Cao, G.; Yang, Z.; Wang, D.; Dubois, D.; Zhou, X.; Graff, G. L.; Pederson, L. R.; Zhang, J.-G. Oriented Nanostructures for Energy Conversion and Storage. *ChemSusChem* **2008**, *1*, 676–697.
7. Pasquier, A. D.; Plitz, I.; Menocal, S.; Amatucci, G. A Comprehensive Study of Li-Ion Battery, Supercapacitor, and Nonaqueous Asymmetric Hybrid Devices for Automotive Applications. *J. Power Sources* **2003**, *115*, 171–178.
8. Conway, B. E. *Electrochemical Supercapacitors—Scientific Fundamentals and Technological Applications*; Kluwer Academic/Plenum Publishers: New York, 1999.
9. Zhang, L. L.; Zhao, X. S. Carbon-Based Materials as Supercapacitor Electrodes. *Chem. Soc. Rev.* **2009**, *38*, 2520–2531.
10. Frackowiak, E. Carbon Materials for Supercapacitor Application. *Phys. Chem. Chem. Phys.* **2007**, *9*, 1774–1785.
11. Khomenko, V.; Raymundo-Piñero, E.; Béguin, F. Optimization of an Asymmetric Manganese Oxide/Actived Carbon Capacitor Working at 2 V in Aqueous Medium. *J. Power Sources* **2006**, *153*, 183–190.
12. Khomenko, V.; Raymundo-Piñero, E.; Frackowiak, E.; Béguin, F. High-Voltage Asymmetric Supercapacitors Operating in Aqueous Electrolyte. *Appl. Phys. A: Mater. Sci. Process.* **2006**, *82*, 567–573.
13. Cottineau, T.; Toupin, M.; Delahaye, T.; Brousse, T.; Bélanger, D. Nanostructured Transition Metal Oxides for Aqueous Hybrid Electrochemical Supercapacitors. *Appl. Phys. A: Mater. Sci. Process.* **2006**, *82*, 599–106.

14. Algharaibeh, Z.; Liu, X.; Pickup, P. G. An Asymmetric Anthraquinone-Modified Carbon/Ruthenium Oxide Supercapacitor. *J. Power Sources* **2009**, *187*, 1640–643.
15. Duffy, N. W.; Baldsing, W.; Pandolfo, A. G. The Nickel-Carbon Asymmetric Supercapacitor-Performance, Energy Density and Electrode Mass Rations. *Electrochim. Acta* **2008**, *54*, 535–539.
16. Qu, Q.; Zhang, P.; Wang, B.; Chen, Y.; Tian, S.; Wu, Y.; Holze, R. Electrochemical Performance of MnO_2 Nanorods in Neutral Aqueous Electrolyte as a Cathode for Asymmetric Supercapacitors. *J. Phys. Chem. C* **2009**, *113*, 14020–14027.
17. Yuan, C.-Z.; Gao, B.; Zhang, X.-G. Electrochemical Capacitance of $NiO/Ru_{0.35}V_{0.65}O_2$ Asymmetric Electrochemical Capacitor. *J. Power Sources* **2007**, *173*, 606–612.
18. Kaempgen, M.; Chan, C. K.; Ma, J.; Cui, Y.; Gruner, G. Printable Thin Film Supercapacitors Using Single-Walled Carbon Nanotubes. *Nano Lett.* **2009**, *9*, 1919–1923.
19. Chen, P. C.; Shen, G.; Sukcharoenchoke, S.; Zhou, C. Flexible and Transparent Supercapacitor Based on In_2O_3 Nanowire/Carbon Nanotube Heterogeneous Films. *Appl. Phys. Lett.* **2009**, *94*, 43113–43115.
20. Wei, M.; Konishi, Y.; Zhou, H.; Sugihara, H.; Arakawa, H. Synthesis of Single-Crystal Manganese Dioxide Nanowires by a Soft Chemical Process. *Nanotechnology* **2006**, *16*, 245–249.
21. Wyckoff, R. W. G. *Crystal Structures*; Interscience: New York, 1968.
22. Li, C.; Zhang, D.; Han, S.; Liu, X.; Tang, T.; Zhou, C. Diameter-controlled Growth of Single-Crystalline In_2O_3 Nanowires and Their Electronic Properties. *Adv. Mater.* **2003**, *15*, 143–146.
23. Xu, C.; Du, H.; Li, B.; Kang, F.; Zeng, Y. Asymmetric Activated Carbon-Manganese Dioxide Capacitors in Mild Aqueous Electrolyte Containing Alkaline-Earth Cations. *J. Electrochem. Soc.* **2009**, *156*, A435–441.
24. Devaraj, S.; Munichandraiah, N. Effect of Crystallographic Structure of MnO_2 on Its Electrochemical Capacitance Properties. *J. Phys. Chem. C* **2008**, *112*, 4406–4417.
25. Prasad, K. R.; Koga, K.; Miura, N. Electrochemical Deposition of Nanostructured Indium Oxide: High-Performance Electrode Material for Redox Supercapacitors. *Chem. Mater.* **2004**, *16*, 1845–1847.
26. Shaijumon, M. M.; Ou, F. S.; Ci, L.; Ajayan, P. M. Synthesis of Hybrid Nanowire Arrays and Their Application as High Power Supercapacitor Electrodes. *Chem. Commun.* **2008**, *20*, 2373–2375.
27. Frackowiak, E.; Béguin, F. Carbon Materials for the Electrochemical Storage of Energy in Capacitors. *Carbon* **2001**, *39*, 937–950.
28. Jurewicz, K.; Frackowiak, E.; Béguin, F. Towards the Mechanism of Electrochemical Hydrogen Storage in Nanostructured Carbon Materials. *Appl. Phys. A: Mater. Sci. Process.* **2004**, *78*, 981–987.
29. Wang, G.-Z.; Zhang, B.-L.; Yu, Z.-L.; Qu, M.-Z. Manganese Oxide/MWNTs Composite Electrodes for Supercapacitors. *Solid State Ionics* **2005**, *176*, 1169–1174.
30. Pasquier, A. D.; Plitz, I.; Gural, J.; Menocal, S.; Amatucci, G. Characteristics and Performance of 500 F Asymmetric Hybrid Advanced Supercapacitor Prototypes. *J. Power Sources* **2003**, *113*, 62–71.
31. Zhang, D.; Ryu, K.; Liu, X.; Polikarpov, E.; Ly, J.; Tompson, M. E.; Zhou, C. Transparent, Conductive, and Flexible Carbon Nanotube Films and Their Application in Organic Light-emitting Diodes. *Nano Lett.* **2006**, *6*, 1880–1886.
32. Hu, L.; Choi, J. W.; Yang, Y.; Jeong, S.; Mantia, F. L.; Cui, L. F.; Cui, Y. Highly Conductive Paper for Energy-Storage Devices. *Proc. Natl. Acad. Sci. U.S.A.* **2009**, *106*, 21490–21494.
33. Lee, S. W.; Kim, B.-S.; Chen, S.; Yang, S.-H.; Hammond, P. T. Layer-by-Layer Assembly of All Carbon Nanotube Ultrathin Films for Electrochemical Applications. *J. Am. Chem. Soc.* **2009**, *131*, 671–679.
34. Kim, D. K.; Muralidharan, P.; Lee, H. -W; Ruffo, R.; Yang, Y.; Chan, C. K.; Peng, H.; Huggins, R. A.; Cui, Y. Spinel LiMnO Nanorods as Lithium Ion Battery Cathodes. *Nano Lett.* **2008**, *8*, 3948–3952.